University of Saskatchewan
Subatomic Physics Internal Report

SPIR 144

Calibration of the 5-paddle Flux Monitor for the ^{209}Bi Compton scattering measurement

Rob Pywell

August 24, 2009

Abstract

The results of the analysis of the calibration of the 5-paddle flux monitor for the June 2009 ^{209}Bi Compton scattering measurement at HIGS are presented.

Contents

1 Introduction

This document describes the calibration of the 5-paddle flux monitor as used in the June 2009 run period at HIGS. During this period Compton scattering measurements performed using a ^{209}Bi target and the HINDA NaI detectors. The 5-paddle photon flux monitor was placed after the target and before a large NaI detector (Molly) that could be moved into the beam for flux monitor calibration runs. The objective of the measurements is to confirm that the efficiency of the flux monitor can be accurately predicted by the simulation.

It is generally more convenient to speak in terms of a Flux Monitor calibration factor f_m, instead of the flux monitor efficiency ϵ_m. These are defined as follows: For the live time of a measurement,

N_γ = Number of gamma rays incident on the monitor,
N_m = Number of measured gamma rays, i.e. the flux monitor counts.

We then define,

$\epsilon_m = N_m/N_\gamma$ = The Flux Monitor efficiency,
$f_m = 1/\epsilon_m$ = The Flux Monitor calibration factor.

2 Experimental Setup

For these measurements all the NIM and data acquisition electronics was located in the HIGS counting room (Keck Laboratory). The the signal cables from the 5 paddle system were patched from the experimental vault to the counting room using RG-8 cables. Many runs to determine the calibration of the monitor were performed at most of the photon energies employed during this running period. For each calibration run, a NaI detector was moved into the beam downstream of the flux monitor, and the target was removed. In addition, the photon beam intensity was reduced by inserting copper absorbers into the beam line before the primary collimator so that the NaI would be able to count individual photons. A schematic of the experimental arrangement is shown in figure 1.

The electronics for the flux monitor is part of a dedicated flux monitoring electronics rack which included other devices such as the 3-paddle system, the deuteron photoneutron system, and the HPGe detector.

The 5-paddles for the flux monitor passed to a QDC with a common gate. Originally the NaI signal was also passed in the same QDC but with a different gate width when NaI events came along. The DAQ was set up so that a threshold was not applied in the QDC so that pedestals values were read out when there was no signal for a particular paddle or the NaI. However, the application of multiple gate widths to the QDC significantly confused the issue when it came to sorting out pedestals and interfered with the cleanness of the spectra. Apparently a long gate from the NaI, which is triggered for all NaI, was often present when there were also signals from the paddles. The most expedient thing to do was to move the NaI to a separate peak-sensing ADC. In the analysis we will see that this creates its own issues, which will be discussed in section 4.

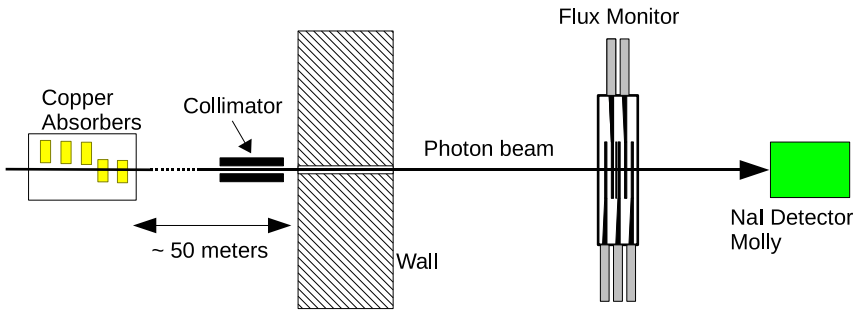

Figure 1: A schematic of the experimental arrangement used to characterize the photon flux monitor (not to scale).

3 Data Taking Procedure

Calibration data was taken at most photon energies during the run. The data taking procedure is different from that described in SPIR-140 [1] and reference [2]. As detailed in those reports, the most difficult quantity to determine was the background count rate in the 5-paddle flux monitor at the low photon rates employed when the copper absorbers are used to reduce the beam intensity. It was found that the background rate, as measured after the beam was turned off, varied according to the time after the beam was off. Therefore a way of determining the background during the time the beam is actually on is required.

As described in SPIR-140 [1] the initial goal is to determine the quantity

$$f'_m = \frac{N_{NaI}}{(N_m - B_m T_{live})} \tag{1}$$

where N_{NaI} is the number of beam photons detected by the NaI detector, which is determined from the integral of the NaI spectrum, N_m is the flux monitor counts during the live time, B_m is the background count rate from the flux monitor in the live time, and T_{live} is the live time for the measurement.

Since B_m is difficult to measure, several runs are taken at different beam rates accomplished by changing the number of copper attenuators. Rearranging the above equation we get

$$\frac{N_{NaI}}{T_{live}} = f'_m \frac{N_m}{T_{live}} - B_m f'_m \tag{2}$$

Therefore we plot the Molly rate N_{NaI}/T_{live} against the 5-paddle flux monitor rate N_m/T_{live} and the slope of a linear fit gives f'_m. This removes the need to determine B_m explicitly. However in the analysis, described in section 5, we do check to see that B_m has a physically reasonable value.

The procedure we used for taking the flux monitor calibration data is reproduced in Appendix A.

Table 1 lists the calibration data taken. The table is presented in chronological order. In the table column 1 is the photon beam energy and column 2 is the data acquisition run number. Column 3 is the date and time at the start of the run. Column 4 is the live time of

the run. Column 5 is the rate in the flux monitor scaler during the live time. and Column 6 is the total rate in the NaI detector during the live time. The total count in the flux monitor scaler during the live time is listed in column 7. Column 8 is the integral of the NaI spectrum which is, of course, recorded during the live time.

Table 1: Flux Monitor (FM) Calibration Runs. The run marked with a $*$ was a background/cosmic ray run with no beam. For the runs marked with a † the Bismuth target was in the beam.

Beam Energy (MeV)	Run	Date/Time	Live Time (s)	FM Rate (Hz)	NaI Rate (Hz)	FM Count	NaI Count
14.7	1059	Jun 2 08:44	526.4	15.8	996	8332	440721
14.7	1060	Jun 2 08:54	341.7	32.2	1928	10994	592446
14.7	1061	Jun 2 09:01	169.0	74.0	4318	12503	676871
15.1	1084	Jun 3 10:29	263.2	16.2	1009	4253	224583
15.1	1085	Jun 3 10:34	166.6	36.2	2120	6032	321613
15.1	1086	Jun 3 10:38	167.0	69.3	4006	11565	627171
15.1	1087	Jun 3 10:42	104.7	126.7	7328	13264	728170
12.0	1103	Jun 3 21:22	141.1	94.6	5506	13353	732777
12.0	1104	Jun 3 21:25	373.7	23.8	1473	8902	486834
12.0	1105	Jun 3 21:32	112.0	87.5	5067	9808	533676
12.0	1106	Jun 3 21:36	250.7	27.6	1694	6920	380096
12.0	1107	Jun 3 21:41	187.2	52.6	3078	9844	534405
13.0	1116	Jun 4 12:41	382.5	26.1	2151	9994	544298
13.0	1117	Jun 4 12:48	97.0	225.9	13547	21910	1205630
13.0	1118	Jun 4 12:51	123.1	69.6	4608	8561	468797
13.0	1119	Jun 4 12:54	287.1	35.4	2684	10153	556930
13.0	1120	Jun 4 13:00	52.0	71.0	4588	3691	197260
13.0	1121	Jun 4 13:02	27.3	243.0	14370	6639	361543
13.0	1122	Jun 4 13:04	85.3	134.3	8265	11458	627529
14.0	1124	Jun 4 14:51	368.7	10.9	1283	4016	213283
14.0	1125	Jun 4 14:58	301.7	27.3	2214	8239	446306
14.0	1126	Jun 4 15:04	53.0	32.2	2514	1707	93681
14.0	1127	Jun 4 15:06	104.8	122.1	7735	12795	714830
14.0	1128	Jun 4 15:08	177.5	58.6	3954	10399	561332
14.0	1129	Jun 4 15:12	290.2	31.8	2445	9230	495014
14.0†	1130	Jun 4 15:18	284.4	25.0	2100	7100	388101
15.8	1143	Jun 4 19:37	472.2	15.6	1535	7356	384271
15.8	1144	Jun 4 19:45	279.7	31.1	2406	8689	464582
15.8	1145	Jun 4 19:51	244.6	37.5	2774	9182	493888
15.8	1146	Jun 4 19:56	134.5	74.3	4874	9998	545977

... continued on next page

Table 1 ... continued from previous page

Beam Energy (MeV)	Run	Date/Time	Live Time (s)	FM Rate (Hz)	NaI Rate (Hz)	FM Count	NaI Count
11.0	1155	Jun 5 10:24	277.2	32.0	2464	8882	472511
11.0	1156	Jun 5 10:30	151.2	58.8	3937	8887	471788
11.0	1158	Jun 5 10:57	49.8	200.9	12158	10005	540858
11.0	1159	Jun 5 10:59	76.3	57.2	3900	4370	235317
11.0	1160	Jun 5 11:02	154.3	68.6	4542	10579	570195
0.0*	1174	Jun 7 12:41	15783.2	0.2	672	2993	–
25.0	1184	Jun 9 15:19	308.8	28.9	2289	8920	492692
25.0	1185	Jun 9 15:25	158.6	62.1	4175	9842	550065
25.0	1186	Jun 9 15:29	147.8	22.6	1990	3336	191218
25.0	1187	Jun 9 15:32	746.0	10.9	1287	8098	442578
17.5†	1194	Jun 9 21:15	303.7	42.6	3074	12944	709864
17.5†	1195	Jun 9 21:21	518.1	19.8	1795	10242	560979
17.5†	1196	Jun 9 21:31	122.9	76.9	4978	9458	516281
17.5†	1197	Jun 9 21:34	524.2	8.1	1135	4266	230074
22.5	1205	Jun 10 14:19	503.0	10.1	1240	5098	276139
22.5	1206	Jun 10 14:29	475.0	21.2	1878	10064	562407
22.5	1207	Jun 10 14:38	343.0	25.6	2141	8797	494750
22.5	1208	Jun 10 14:45	184.2	55.1	3777	10154	565348
22.5†	1210	Jun 10 14:49	245.1	42.2	3048	10348	571772
18.5	1216	Jun 10 19:20	541.9	15.5	1544	8411	458246
18.5	1217	Jun 10 19:30	220.6	31.9	2510	7047	396430
18.5	1218	Jun 10 19:35	155.1	61.8	4205	9582	536679
18.5†	1219	Jun 10 19:39	181.5	48.2	3407	8741	484774
19.5	1234	Jun 11 15:27	404.8	13.4	1431	5406	297618
19.5	1235	Jun 11 15:35	154.6	69.7	4625	10779	602692
19.5	1236	Jun 11 15:38	395.9	37.2	2764	14729	814899
19.5†	1237	Jun 11 15:46	362.7	28.2	2252	10213	558646
21.5	1242	Jun 11 20:08	579.1	17.5	1665	10136	561333
21.5	1243	Jun 11 20:19	1221.8	8.2	1136	10078	545025
21.5	1244	Jun 11 20:41	230.4	45.2	3272	10417	591044
21.5†	1245	Jun 11 20:46	305.3	33.9	2643	10364	589652

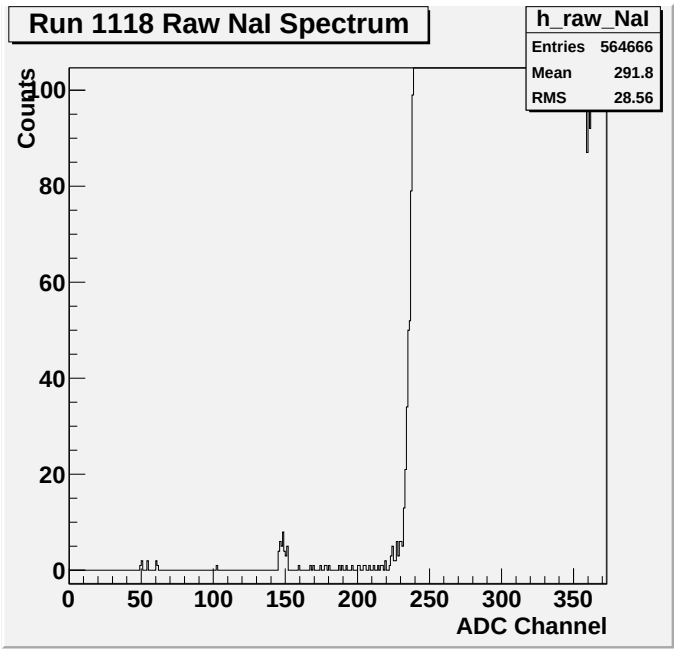

Figure 2: The low pulse height part of a raw NaI spectrum. A pedestal peak can be seen clearly at channel 147.

4 The NaI Spectrum

We need to integrate the NaI spectrum to determine N_{NaI} for equations 1 and 2.

The first step is to make an energy calibrated NaI spectrum. Even though a peak-sensing ADC is used there is still a pedestal in the NaI spectrum when a gate is applied and there is no signal. Normally in the current set-up a gate is only sent to the ADC if there is a signal above the NaI discriminator. However, very infrequently, a noise spike will trigger the discriminator when there is no NaI signal. This gives rise to a pedestal peak in the raw NaI spectrum. An example of finding this pedestal value is shown in figure 2.

From the simulation we have observed that the main peak of the spectrum is very close to the beam energy. Therefore, for simplicity we set the peak channel, after pedestal subtraction, equal to the beam energy as set by the HIGS operators. We do have NaI calibration points with sources at various times. These source calibrations did, in general, agree with beam energy. However, there were small drifts in the NaI gain over time. For this reason we simply set the peak channel equal to be beam energy for each set of runs.

An example of an energy calibrated NaI spectrum is shown in Figure 3. The red line shows the GEANT4 simulation at this energy. Details of the simulation are described in the section 6. In general the GEANT4 simulation agreed very well with the measured spectra in the main beam energy peak.

The bottom graph in Figure 3 shows the full measured spectrum on a log scale. Note that there are pile-up events extending to double the beam energy.

We would expect two possible contributions to these pile-up events. There will be some

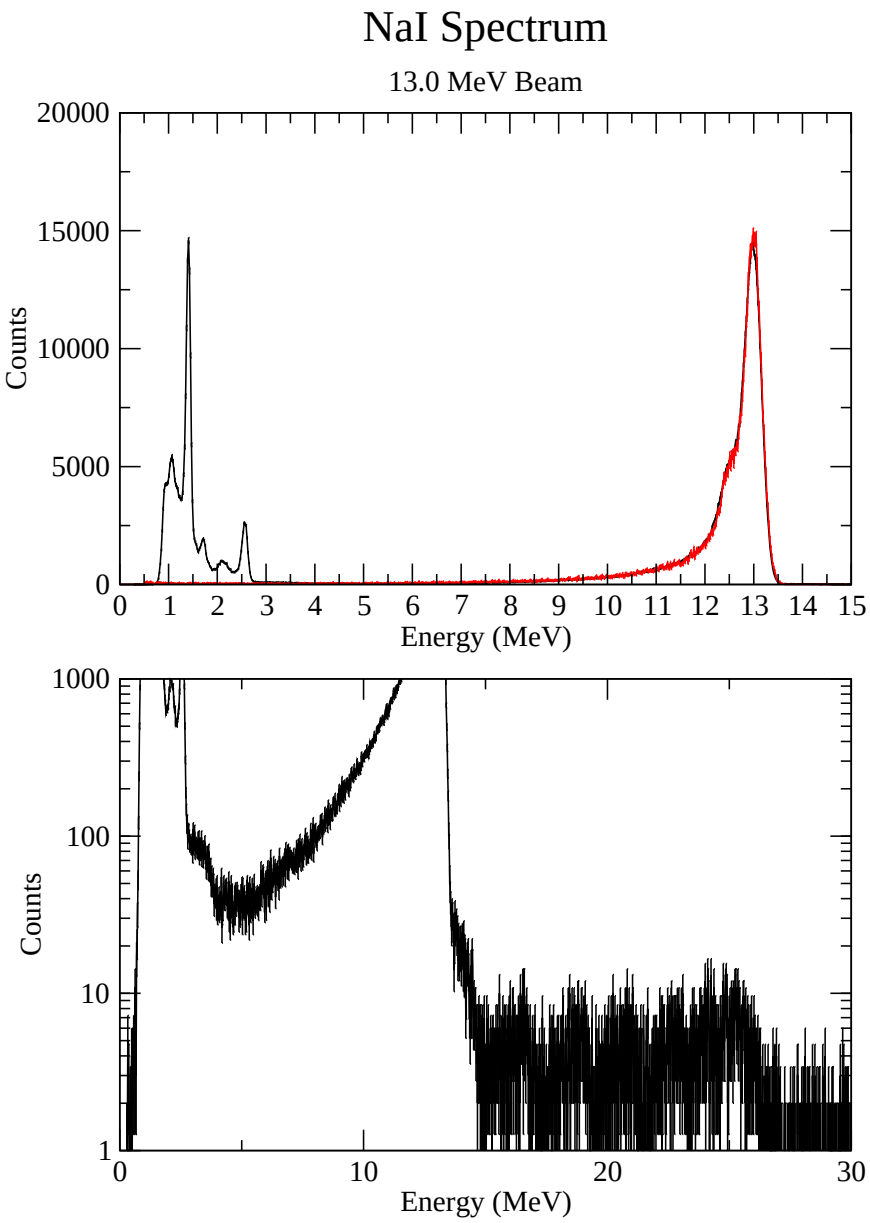

Figure 3: The measured NaI spectrum at a beam energy of 13 MeV and a NaI count rate of about 2000 Hz is shown in black. The red line in the upper graph shows the GEANT4 simulation.

due to a coincidence between a background or cosmic ray photon and a beam photon. Such pile-up will appear in the spectrum at energies within an MeV or two above beam energy peak. There will be some that are due to a coincidence between two beam photons in the same beam bunch. Such pile-ups would mostly appear at an energy of about two times the beam energy. However, an examination of the spectra reveals that there is a third contribution.

For example, in run 1116, which is shown in Figure 3, the photon rate during the live time was about 2100 s^{-1}. At this rate the simulation shows that the fraction of pile up events is about 0.02%, and nearly all of these should be at an energy of about 2 times the beam energy. From the actual measured NaI spectrum we see that the fraction of pile up events is about 0.5%, most of which are at energies distributed between the beam energy and 2 times the beam energy. This pile-up appears as multiple peaks, the shapes of which mimic the shape of the main beam energy peak.

These pile-up events appear to be due to the fact that the NaI amplifier pulse integration shaping time is long. This allows photons from multiple beam bunches to be included in the integration. A photon arriving in different beam bunches after the initial photon will add to the pulse in different ways. This gives rise to the discrete set of energies in the pile-up part of the spectrum. Figures 4, 5, and 6 show the NaI spectrum with an expanded vertical scale for different beam energies. It can be seen that the shape of the pile-up part of the spectrum is different at different beam set-ups. This is consistent with earlier observations that the number of photons in each bunch is not necessarily constant. At different beam set-ups there can be more, less or even zero photons in bunches neighboring a particular bunch.

Another statistic that is consistent with this observation is the difference between the live-time derived from a constant rate signal such as the bunch rate (BPM) and a signal related to the beam flux such as the flux monitor counts. For example, in run 1126 the live-time from the bunch rate is 91.3%, while the live-time from the 5-paddle counter is 86.7 $\pm$ 0.8%. If the beam intensity is higher at some times than at others, the NaI is most likely to receive a hit at a high rate time, thus causing the system to go dead. Therefore the 5-paddle counter is live preferentially during the lower rate period, and so the live-time 5-paddle counts divided by the real-time 5-paddle counts will yield a lower "live time percentage" than that derived from the BPM. [This is the reason why it is vital to record important quantities in live-time gated scalers, instead of correcting a real-time quantity with a live fraction measured using a clock. We have come across this effect before in the tagged photon work at SAL for non-100% duty-factor beams, and the effects have been confirmed with time-sequence simulations.]

The question we need to answer now is "what energy range of the NaI spectrum should we integrate to find N_{NaI}?" Should we include the pile-up events or not? Let us examine the different types.

1. A beam photon in coincidence with a background photon or cosmic ray, should be included since there is one beam photon that could have been detected by the flux monitor.

2. Two beam photons in the same bunch should count double since either photon could have been detected by the flux monitor.

3. Two beam photons in different bunches.

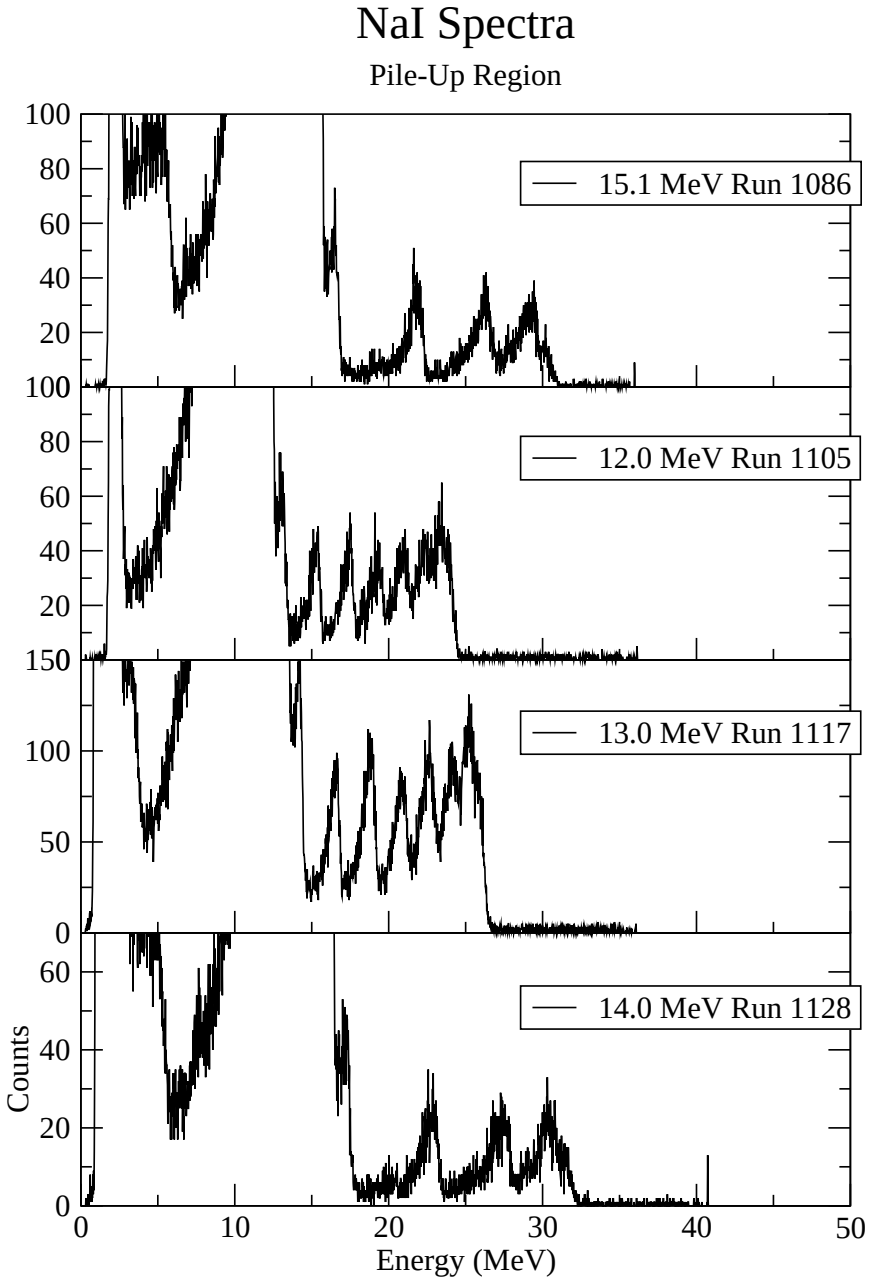

Figure 4: The NaI spectrum for various energies shown on an expanded vertical scale.

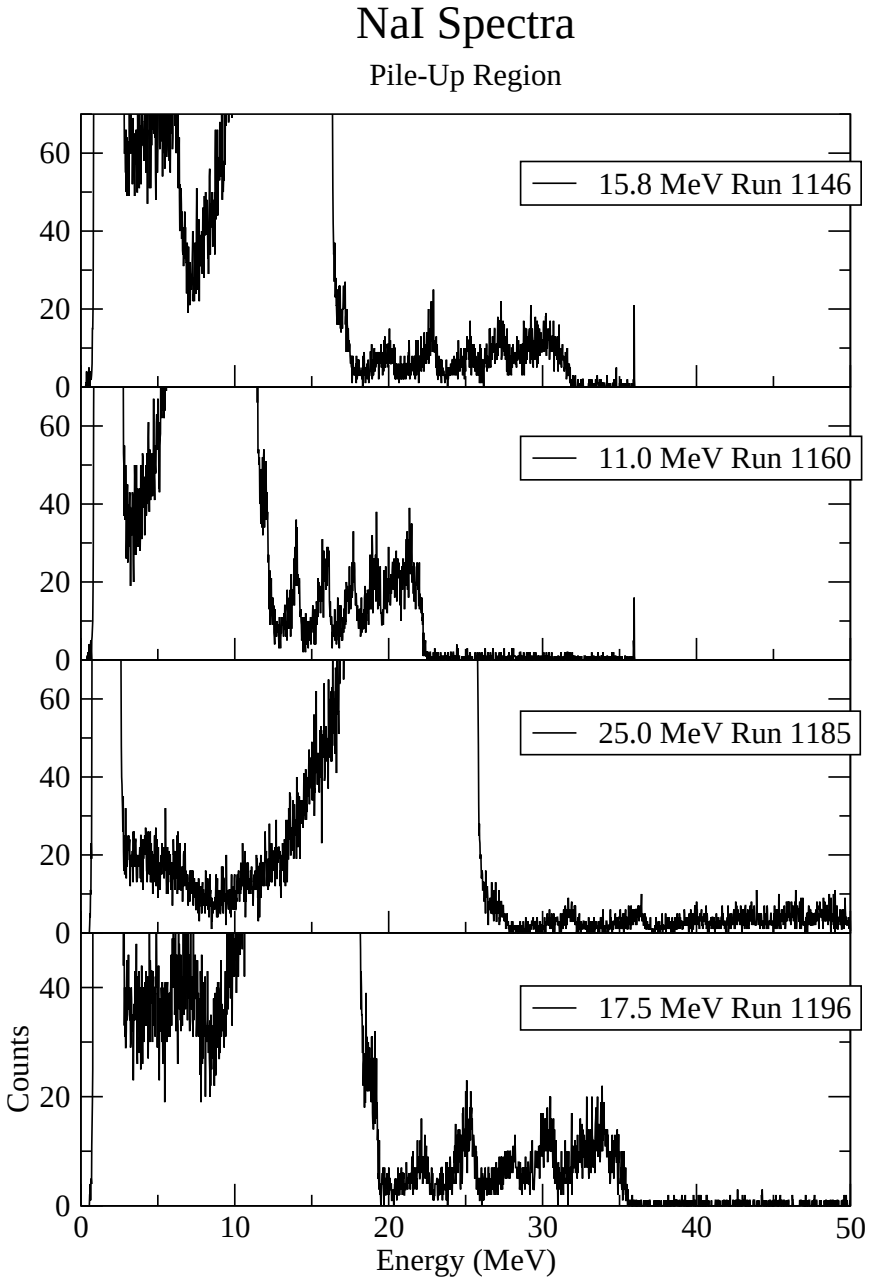

Figure 5: The NaI spectrum for various energies shown on an expanded vertical scale.

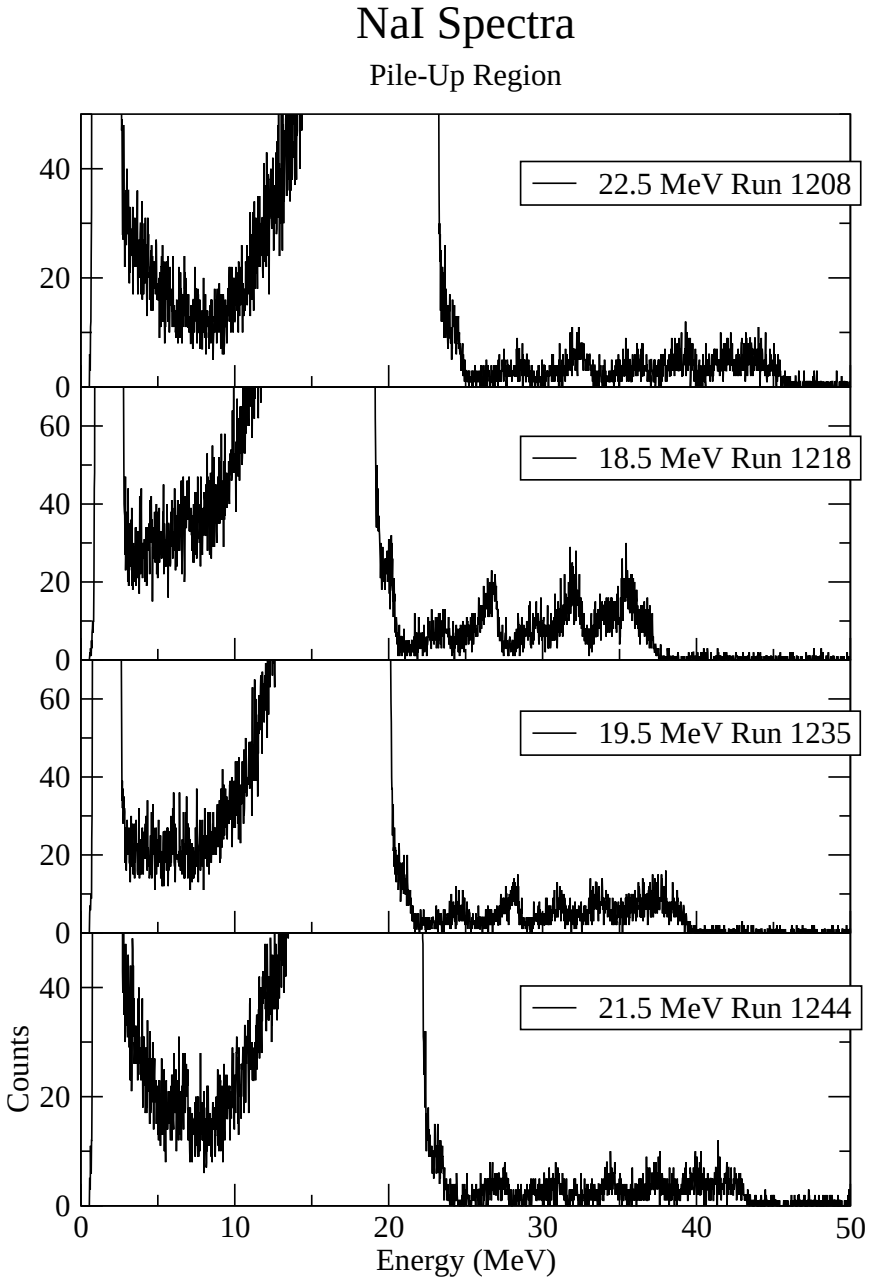

Figure 6: The NaI spectrum for various energies shown on an expanded vertical scale.

We might be tempted to assume that type 3 events should be counted double like type 2 events. However, when the discriminator fires with a photon from a particular bunch, it opens a gate to the NaI ADC. This brings up the inhibit and should stop the live time gated scaler counting the flux monitor signals as it should. Thus photons in later bunches will not be counted by the flux monitor and therefore type 3 pile-up events should be counted only once in the NaI integral.

To further investigate the pile-up question we examine two runs taken at different rates. Figure 7 shows the spectrum at 14 MeV for run 1128, taken at a NaI live-time rate of 3954 Hz, compared to run 1124, taken at a NaI live-time rate of 1283 Hz. The spectrum for run 1124 has been scaled up by the ratio of the flux monitor counts in run 1128 to the counts in run 1124. We see that in the main beam energy peak the spectra agree very well, while the pile-up region is quite different. From this we see that the small peak just above the main beam energy peak at about 15.3 MeV is part of the multi-bunch pile-up spectrum. It it were due to type 1 pile-up events, it would have scaled with beam photon rate. (This is because, given that a beam photon has hit the NaI, the probability that a background photon hits at the same time should be constant, since the background rate is constant.) The tail of this peak extends down into the main beam energy peak.

To account for these pile-up effects as accurately as we can we integrate the NaI spectrum over two energy ranges. First, we choose an integration range that includes the main beam energy peak and rejects as much of the pile-up region as possible. We call this integral N_b'. Second, we integrate from the maximum energy included in N_b' to an energy that includes all the pile-up events. We call this integral N_p'. We choose the lower limit for the N_p' to be 8 MeV. As can be seen from figure 7 this lower limit rejects most of the features in the room background spectrum. Some photons will be rejected because of this lower limit. However, we apply the same lower limit when integrating the GEANT4 simulated NaI spectrum.

The sum $N_b'+N_p'$ will include all the type 1, 2 and 3 events. However we noted that type 2 event should count double. Therefore we need to make a correction by adding as estimate for the number of type 2 events. Before making this estimate we apply a background correction to N_b' and N_p'.

Even in the integration range chosen there will be some background events. These will mostly be due to cosmic rays since the 8 MeV lower limit rejects most of the room radioactivity. Run 1174 was a very long background run. This run can be used to estimate this cosmic ray rate. Figure 8 shows the background spectrum. Because of the varying upper limit of the integration ranges we need to find a function that will allow us to calculate the background at each energy.

We fit this spectrum between 8 MeV and 34 MeV with a function of the form

$$\frac{\mathrm{d}^2 B_{NaI}(E)}{\mathrm{d}E\mathrm{d}T_{live}} = a_0(1 + a_1 E^{-1} + a_2 E^{-2}) \tag{3}$$

with

$$a_0 = 5.642 \times 10^{-2}\ \text{Counts} \cdot \text{MeV}^{-1} \cdot \text{s}^{-1}$$
$$a_1 = 1.629 \times 10^{1}\ \text{MeV}$$
$$a_2 = 3.784 \times 10^{2}\ \text{MeV}^2$$

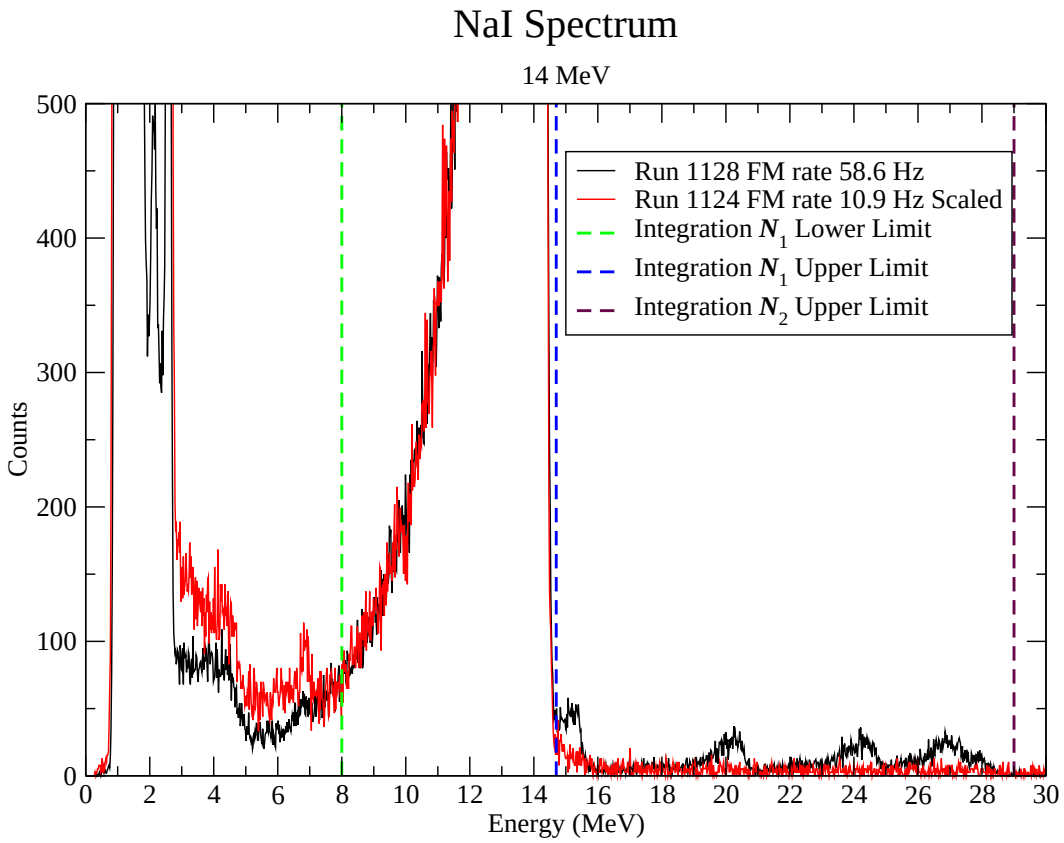

Figure 7: The NaI spectrum at a beam energy of 14 MeV taken at two different beam rates. The spectrum for run 1124 has been scaled up by the ratio of the flux monitor counts in run 1128 to the counts in run 1124.

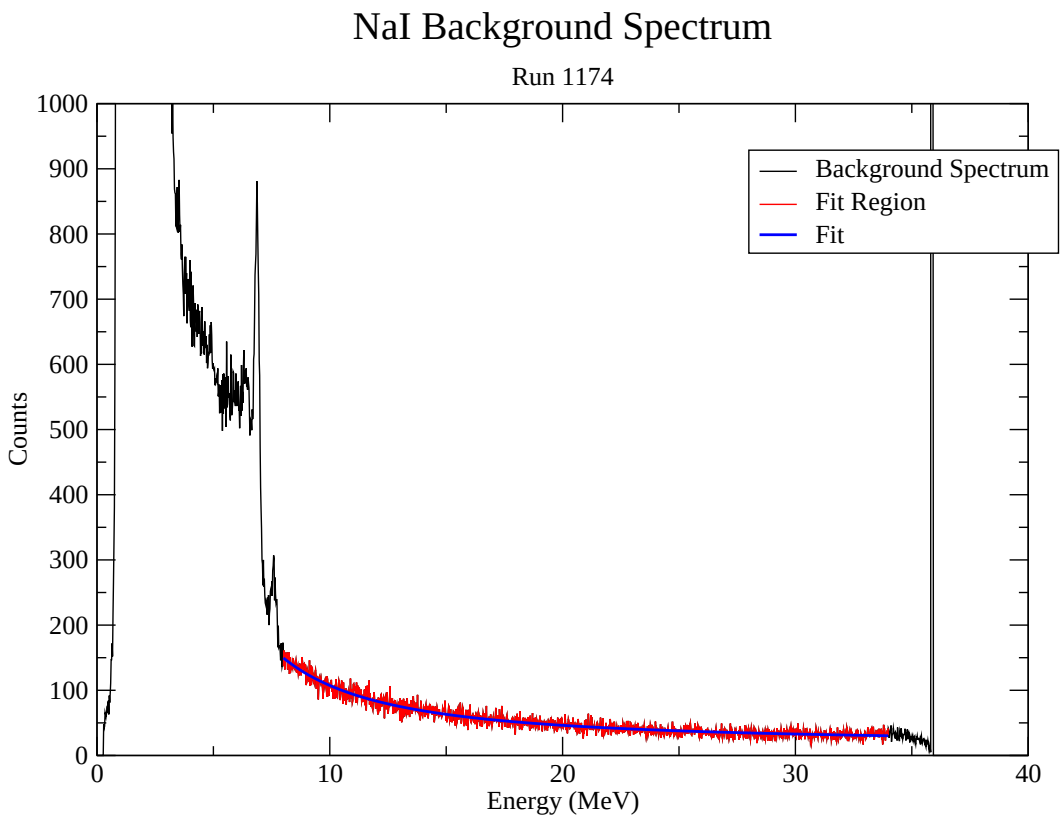

Figure 8: The NaI background spectrum from run 1174. The fit is to the region between 8 MeV and 34 MeV.

We use this formula to calculate the background in the integration range using the live-time for the measurement. If the NaI energy spectrum is binned in bins of width ΔE, and the live time of the measurement is T_{live}, then

$$N_b = N_b' - \sum_{E_i=E_{min}}^{E_{max}} \frac{\mathrm{d}^2 B_{NaI}(E_i)}{\mathrm{d}E \mathrm{d}T_{live}} \Delta E T_{live} \tag{4}$$

and similarly for N_p.

We now make an estimate of the number of type 2 pile-up events N_2. The average number of photons per bunch is, to first order, estimated by $\mu = N_b/B$, where B is the number of bunches during the live time. (This first order estimate ignores the fact that μ may not be constant from bunch to bunch.) From Poisson statistics the number of events with one photon in a bunch will be

$$N_1 = B\mu e^{-\mu} \tag{5}$$

and the number with two photons in a bunch is

$$N_2 = B\frac{\mu^2}{2} e^{-\mu} \tag{6}$$

Since at the photon rates employed for these measurements, μ is very small, we can make the approximation $e^{-\mu} \approx 1$, so $N_1 \approx N_b$. Therefore, combining the above two equations,

$$N_2 = \frac{\mu}{2} N_1 \approx \frac{N_b^2}{2B} \tag{7}$$

As well, since μ is small, we neglect events with more than 2 photons per bunch.

Finally, the corrected number of photons detected by the NaI detector is

$$N_{NaI} = N_b + N_p + N_2 \tag{8}$$

The "NaI Count" in table 1 is N_{NaI} after these corrections have been applied.

The background correction is at most 0.7% for the very lowest rate measurement but is more typically less than a 0.2% correction. The type 2 pile-up correction is at most a 0.05% correction for the rates included in the analysis. Therefore uncertainties in both these corrections will contribute very little to the overall uncertainty of the measurements. On the other hand N_p contributes up to a 1.8% of N_{NaI}. The contribution varies considerably with the beam set-up.

The largest uncertainty in this analysis is the assumption that, when a hit to the NaI is recorded, the inhibit comes up soon enough to prevent photons in later bunches being recorded by the flux monitor. This needs to checked more precisely by observing the signals. If this is not the case the error in N_{NaI} introduced is likely to be less than about 1%.

It would be better to minimize the multi-bunch pile-up effects. In the flux measurements taken in September/October 2008 a QDC was used instead of an ADC. This minimized the multi-bunch pile-up, with at most 2 'extra' peaks observed in the spectrum instead of up to 7 or 8 in these measurements. The pile-up region of the NaI spectrum contributed less than

0.4% to N_{NaI} in the 2008 measurements. We therefore recommend that a QDC be used for future measurements.

In the simulation, to which we are trying to compare these measurements, only one photon is simulated at a time. Therefore, there are no pile-ups in the simulation and so the upper limit on the integration is not critical as long it includes the main peak. The lower limit for integrating the simulated spectrum is set to 8 MeV as it is for the measurement.

5 Measured Calibration Factor

Following the procedure used for the analysis of the 2008 data [1] we begin by calculating the 'measured calibration factor' f'_m, which was define in Equation 1. N_{NaI} is calculated as described in section 4.

To determine f'_m we calculate the NaI live-time rate N_{NaI}/T_{live} and the 5-paddle live-time rate N_m/T_{live}. For each energy we fit a straight line according to equation 2 to extract f'_m and B_m, the background rate in the 5-paddle monitor. Because there are errors on both the dependent and independent variables in the straight line fit the chi-squared fit becomes a nonlinear problem. Therefore a simple search algorithm was used to minimize the chi-squared (see for example [4]).

In the fit both f'_m and B_m are allowed to vary. However, we know that B_m cannot be negative. Indeed it would be non-physical for it to be too small. Figure 9 shows the value of B_m found by the best fit for each energy if there is no restriction placed on possible values. The average value of B_m from this unrestricted fit is $0.39 \pm 0.10\ s^{-1}$.

The background rate determined from the long background run taken on the Saturday afternoon, long after the beam had been in the room, was $0.190 \pm 0.003\ s^{-1}$. Since this would be a good estimate of the steady state room background and cosmic ray rate, it would seem reasonable to expect that this would be a bare minimum background rate possible when the beam is on.

Although previous evidence [1] indicates that the background rate can vary with time after the full intensity beam is turned off. However, the information in figure 9 provides no clear evidence that B_m, measured during the low intensity beam on time varies from run to run. We therefore fix the background rate at $B_m = 0.39 \pm 0.10\ s^{-1}$ for all energies, and determine the f'_m values using this value.

A distinct possibility is that B_m varies with time after the beam intensity is reduced by inserting collimators. This means that different points used in the straight line fit at each energy could be affected differently by background. This could bias the fit. Possible effects such as these need to be investigated in later measurements.

The measured calibration factor calculated using the above procedure are plotted in figure 10.

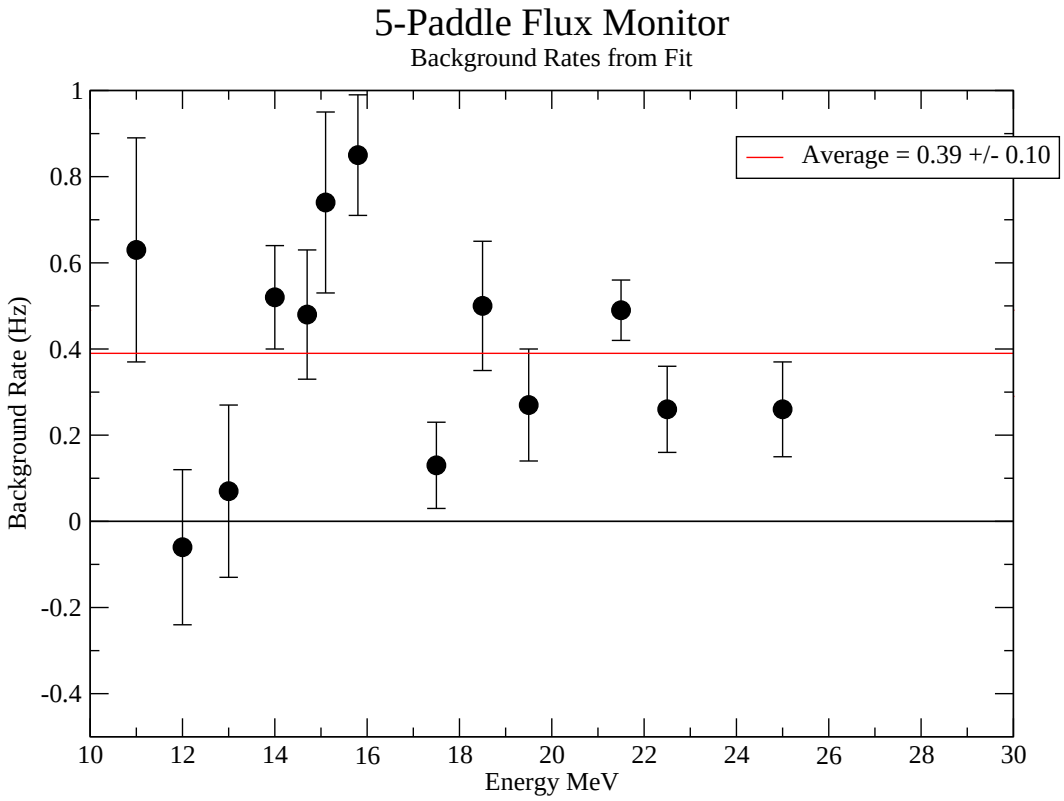

Figure 9: The 5-paddle flux monitor background rates determined from an unrestricted linear fit at each energy.

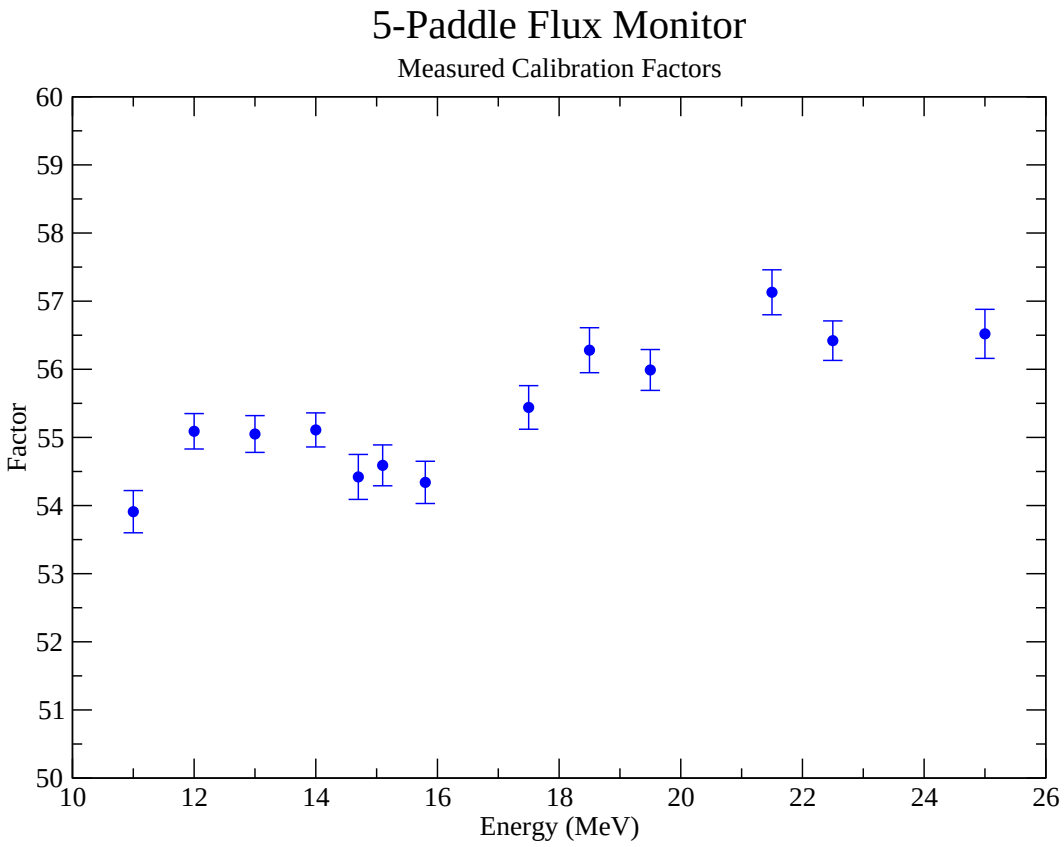

Figure 10: The measured calibration factors for the 5-paddle flux monitor.

6 GEANT4 Simulation

A GEANT4[3] simulation of the experimental arrangement including the flux monitor and the NaI detector has been developed. The simulation has been improved in a number of ways from that which was described in reference [1]. In this section we will only describe these changes.

A couple of simple errors were noted. First, it was found that the dimensions of the NaI detector used in the simulation was in error. Correcting this resulted in an excellent fit for the shape of the NaI spectrum to the measured shape. Second, there was a detector construction error which meant that a small part of the (incorrect dimensioned) NaI crystal was not included in the simulation. Making these correction made a negligible difference to the results. This was confirmed by reanalyzing the data in [1].

A major improvement in the simulation was the inclusion of a more realistic energy spread for the incident photon beam. A good approximation for the gamma-ray photon energy when $\gamma = E_e/m_e c^2 \gg 1$ and the gamma-ray is scattered at a small angle θ to the initial electron direction, is [5]

$$E_\gamma(\theta) \approx \frac{4\gamma^2 E_\lambda}{1 + (\gamma\theta)^2 + 4\gamma E_\lambda/m_e c^2} \tag{9}$$

where m_e is the electron mass, E_e is the initial energy of electron and E_λ is the FEL photon energy which is related to its wavelenght by $E_\lambda = hc/\lambda$.

When the gamma rays pass though a collimator of diameter d, at a distance $L \approx 60\ m$ from the gamma-ray source point, the maximum angle is $\theta_{max} = d/2L$. Thus the gamma-ray energy ranges between E_{max} at $\theta = 0$ to E_{min} at θ_{max}. Assuming a uniform gamma-ray intensity across the collimator the mean energy is given by

$$\begin{aligned} \bar{E} &= \int E_\gamma(\theta) dA / \int dA \\ &= \frac{4E_\lambda}{\theta_{max}} \left[\ln\left(\theta_{max}^2 + \frac{1}{\gamma^2} + \frac{4E_\lambda}{\gamma m_e c^2}\right) - \ln\left(\frac{1}{\gamma^2} + \frac{4E_\lambda}{\gamma m_e c^2}\right)\right] . \end{aligned} \tag{10}$$

Calculating this mean energy for various values of the parameters we find that to a good approximation

$$\bar{E} \approx (E_{min} + E_{max})/2 . \tag{11}$$

We define the energy spread by

$$\Delta E = (E_{max} - E_{min})/2 . \tag{12}$$

To simplify input to the simulation we input only $\bar{E}$ and ΔE. Then using the collimator diameter the code will calculate the appropriate parameters for equation 9. For each event in the simulation a random position within the collimator opening is chosen. This then defines θ, and therefore E_γ through equation 9. We determine the appropriate input value of ΔE by direct calculation using equation 9. Using θ_{max} set by the collimator diameter and E_λ set my the mirror selection, we vary the electron energy (i.e. γ) until we match the gamma-ray

beam energy. We assume that this angular dependence is the major contribution to the gamma-ray beam energy spread.

The simulation was also modified to allow adjustment of the NaI resolution parameter. If E_{dep} is the energy (in MeV) deposited in the NaI crystal, the pulse height recorded in the ADC is

$$E_{ADC} = E_{dep} + G(\sigma_{light})\sqrt{E_{dep}} + G(\sigma_{noise}) \tag{13}$$

where $G(\sigma)$ is a Gaussian distribution of energies centered on zero with a standard deviation σ. Using the above procedure for determining ΔE we find a good fit to the NaI spectra for all energies using $\sigma_{light} = 0.042$ MeV and $\sigma_{noise} = 0.003$ MeV.

Other improvements to the simulation include the ability to change the resolution parameters for each scintillator paddle without recompiling.

A copy of the GEANT4 flux monitor simulation application is available at
`http://nucleus.usask.ca/ftp/pub/rob/flux-1.1.tgz`
The application works with Geant4.8.1.p01. A version that will work with latter releases of GEANT4 will be forthcoming. The application requires the packages "LightOutput" available at
`http://nucleus.usask.ca/ftp/pub/rob/LightOutput-1.0.tgz`.
If output in Lucid[6] format is desired the package "G4Lucid" available at
`http://nucleus.usask.ca/~ward/G4Lucid/index.html`
will also be needed. (The G4Lucid package also requires Lucid to be installed on your system.)

7 Simulation Input Parameters

We now need to establish the input parameters to the simulation appropriate to the current experimental setup, namely the energy threshold for each paddle. From the simulation we can see that the single minimum ionizing peak for each paddle is at the following energies:

Paddle 0, 362 keV;
Paddle 1, 336 keV;
Paddle 2, 336 keV;
Paddle 3, 391 keV;
Paddle 4, 351 keV.

(The peaks are not all at the same energy since the paddles have different thicknesses.)

A simple peak fitting routine was used to find the channel number of the first peak in the paddle spectra for all the calibration runs. These are plotted in figure 11. It can be seen the peak positions, and therefore the gain of each paddle, is approximately constant over the run period. Small changes in gain can be seen for paddles 3 and 4.

The paddle spectra which are accumulated only when the latch for that paddle is set, indicating that the signal was above the discriminator threshold, were examined to determine the threshold energy for each paddle. An example of such a set of spectra is shown in figure 12 for run 1084.

A simple code was also written to find the channel number with the greatest slope in these spectra. This provides a crude estimate of the threshold channel number of each paddle for all runs. because of statistics it was not possible to obtain a value for all cases. Nevertheless the results, which are shown in figure 13, give sense of how stable the threshold channel was during the run period. The horizontal dashed lines in the figure is the channel number for the threshold as estimated by eye from the long background/cosmic ray run number 1174, where the threshold is much easier to see. It can be seen that the threshold is quite constant throughout the run period and threshold channel determined from run 1174 is as good an estimate as we can get.

Using the threshold channel and the gain determined from the peak channel the threshold energies can be calculated. The small gain shifts for paddles 3 and 4 seen in figure 11 result in only at most a 2 keV shift in the threshold energy. In any case the flux monitor efficiency is very weakly dependent on the threshold for paddle 3 and 4. Therefore the average value of the threshold energy was used for all energies in the simulation. The threshold energies used are:

Paddle 0, 270 keV;
Paddle 1, 100 keV;
Paddle 2, 81 keV;
Paddle 3, 78 keV;
Paddle 4, 108 keV.

The simulation was run for all energies in this run period.

Figure 14 shows the simulated paddle spectra compared to the measured paddle spectra for a beam energy of 15.8 MeV. The spectra for paddles 0 and 1 are for the condition that

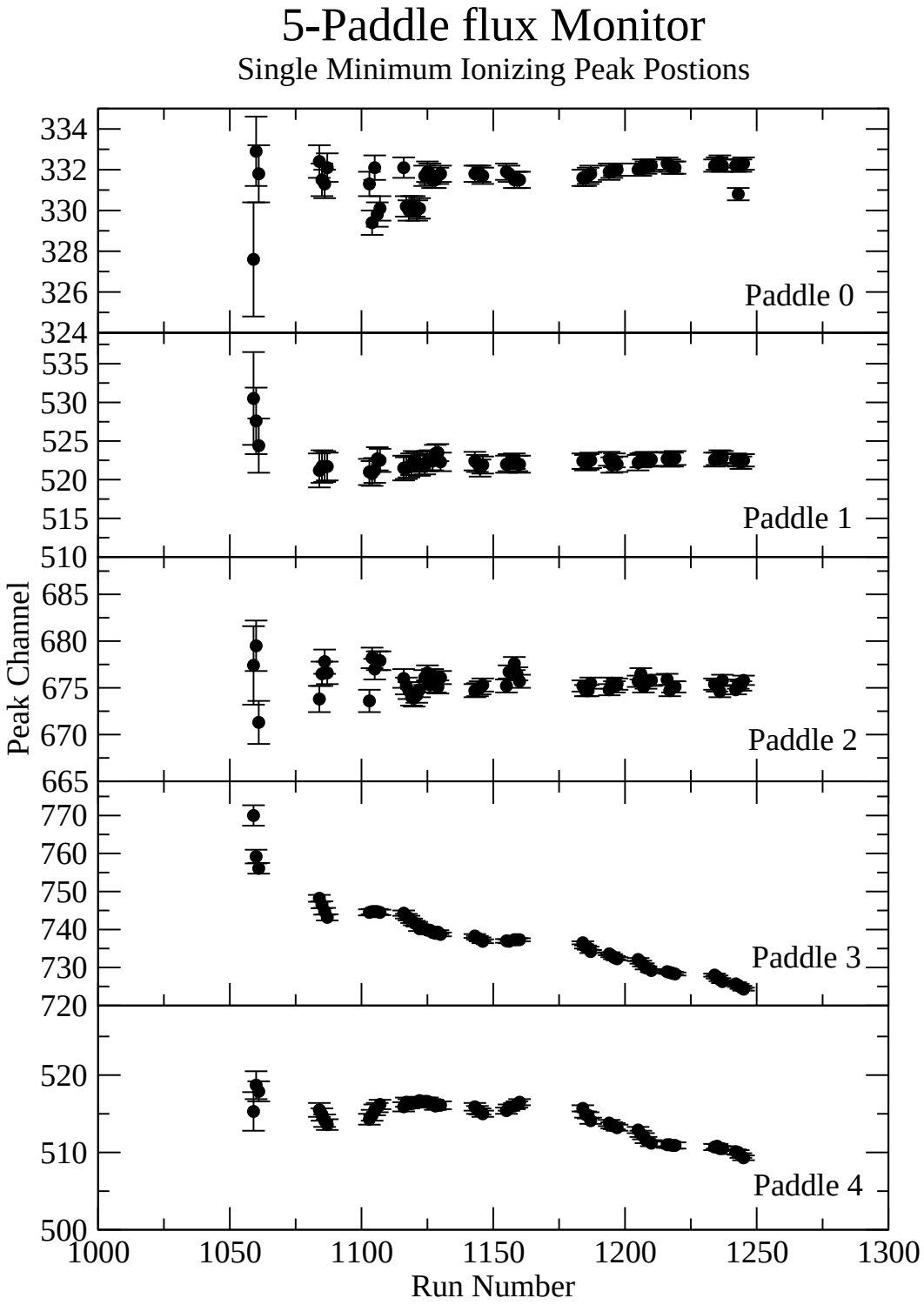

Figure 11: The channel number for the first peak in the paddle spectra for all the calibration runs.

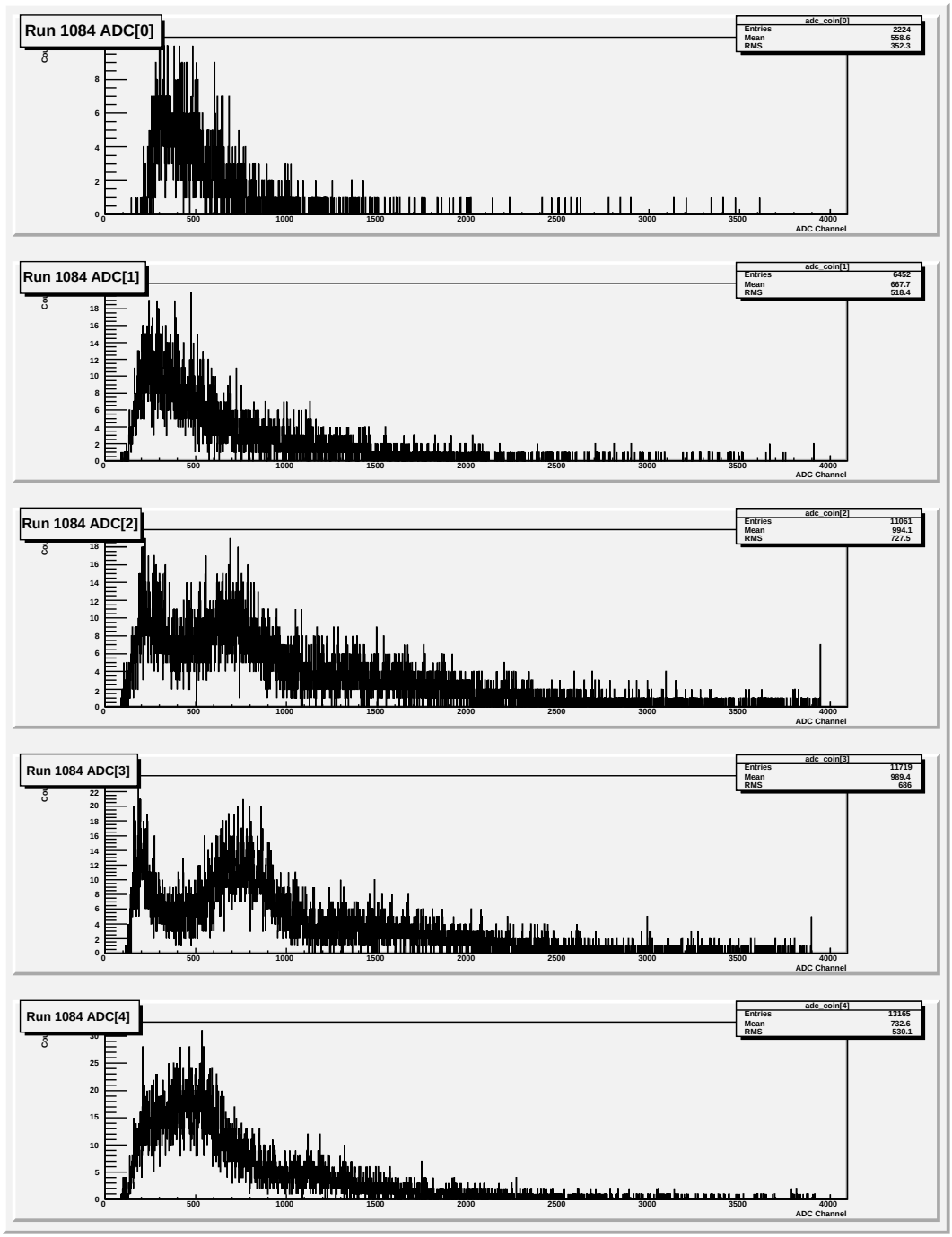

Figure 12: The paddle spectra which are accumulated only when the latch for that paddle is set, indicating that the signal was above the discriminator threshold.

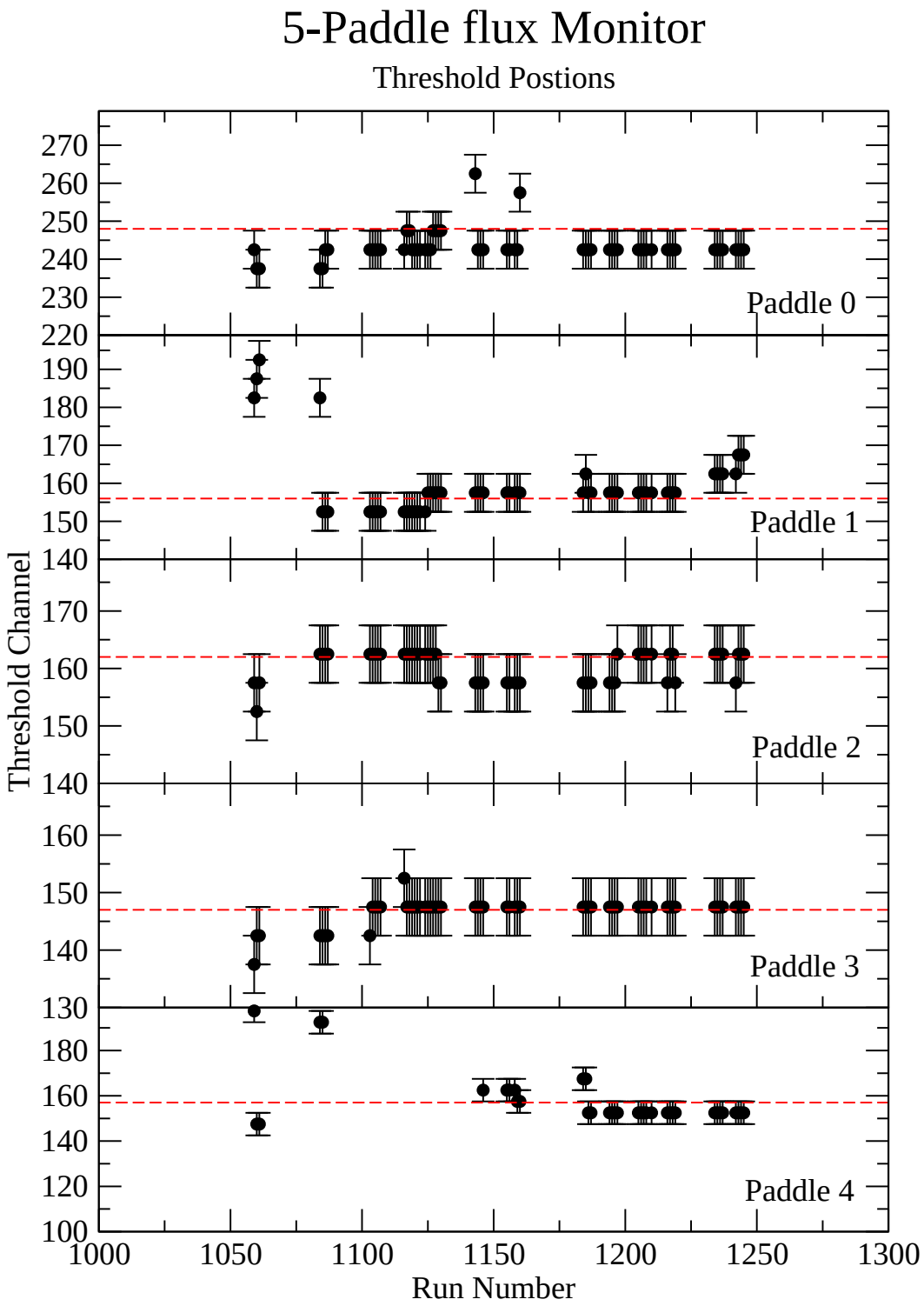

Figure 13: The channel number of the threshold for each paddle for each run. This was estimated using a simple slope finding code. The dashed lines indicate the threshold channel number estimated from the long background/cosmic ray run number 1174.

there is a coincidence between paddles 0, 1 and 2. The spectra for paddle 2, 3 and 4 are for the normal condition for a hit in the flux monitor, i.e. a coincidence between paddles 2, 3 and 4 in anti-coincidence with paddle 2. It can be seen that there is quite good agreement between the measured and simulated spectra.

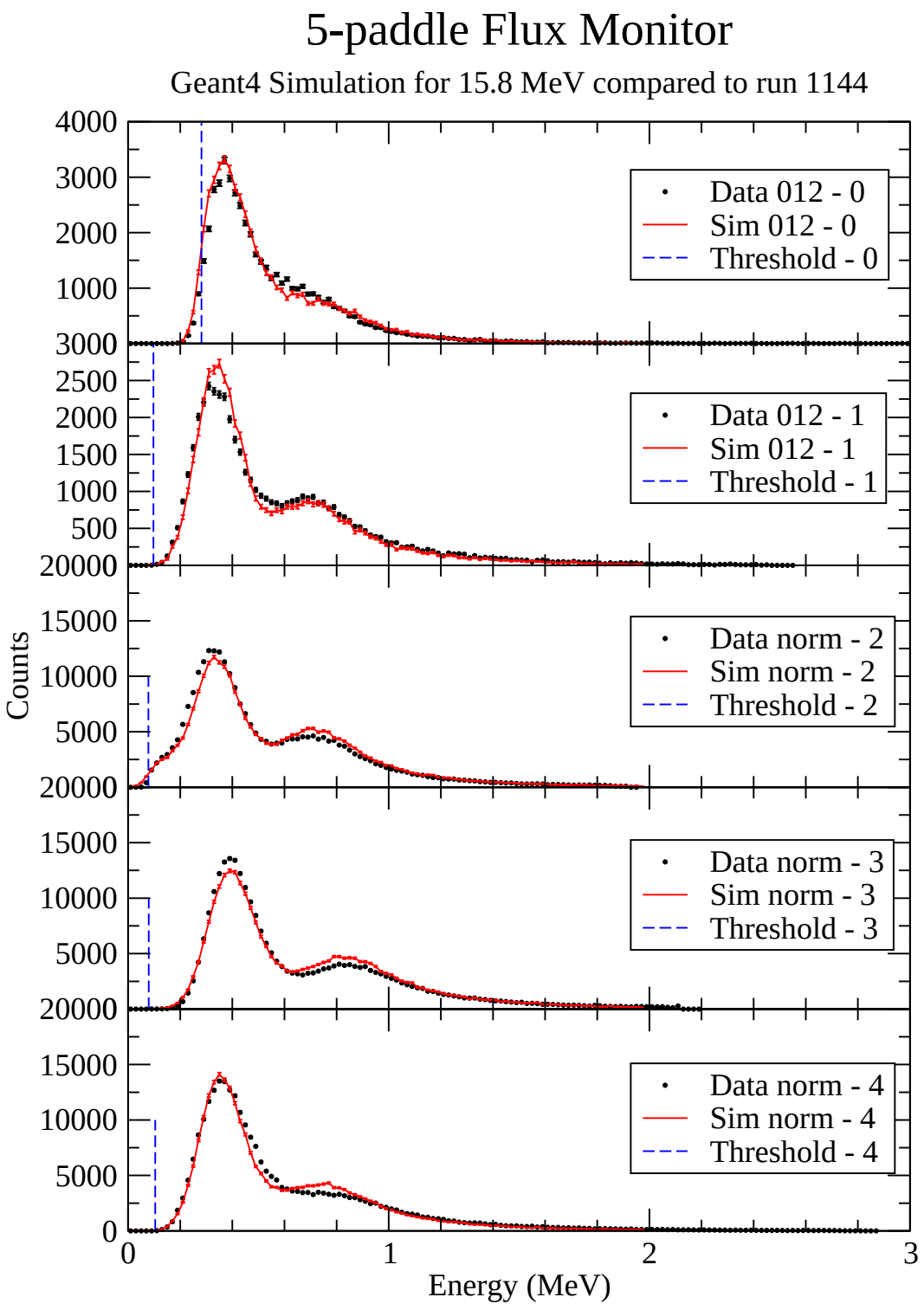

Figure 14: Spectra from the 5 paddles in the flux monitor compared to the simulation for a beam energy of 15.8 MeV.

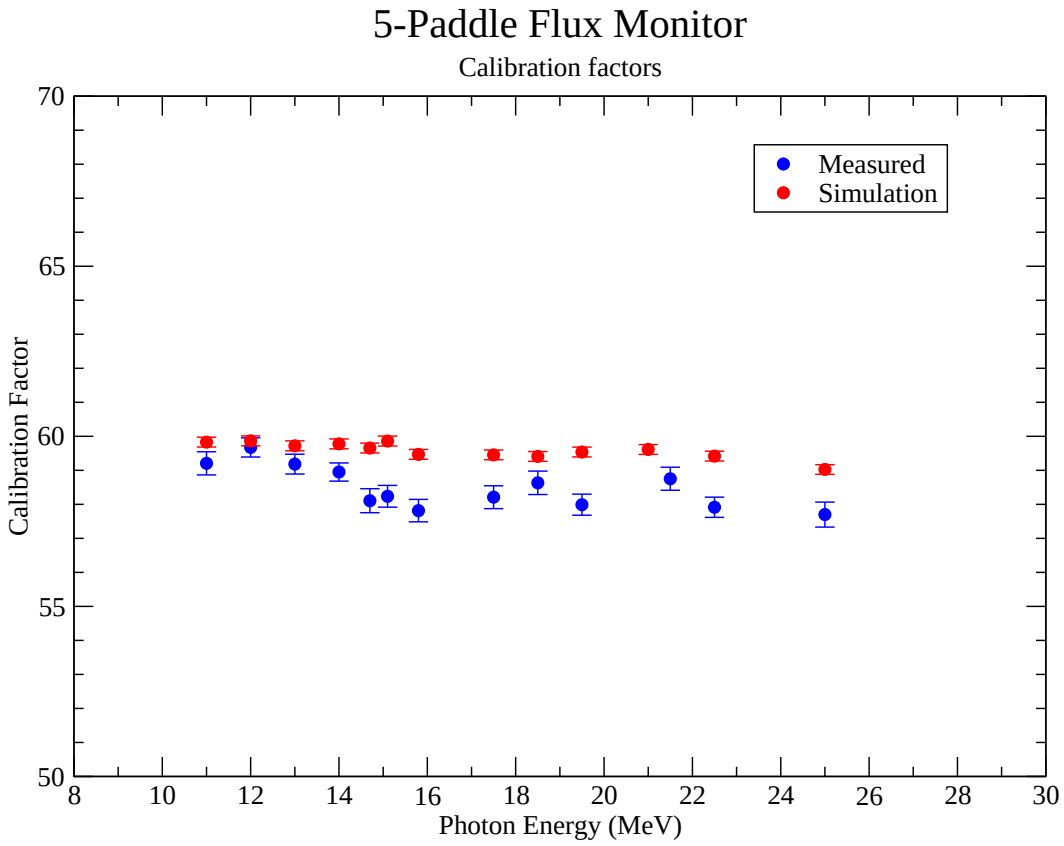

Figure 15: The measured calibration factors, after correction, compared to the simulated calibration factors.

8 Absorption Correction

The measured calibration factor f'_m is not equal to the true calibration factor f_m because not all gamma rays incident on the flux monitor reach, and are detected by, the NaI detector. The correction factor, defined by

$$c_{abs} = N_\gamma / N_{NaI}. \tag{14}$$

is determined from the simulation for each energy.

The true calibration factor is then given by

$$f_m = c_{abs} f'_m \tag{15}$$

The true calibration factor can also be calculated from the simulation

Applying the correction factors to the measured calibration factors plotted in figure 10 we obtain the true measured calibration factor f_m. These are plotted, along with the calculated calibration factors, as a function of energy in figure 15.

It can be seen from figure 15 that there is some disagreement between the measured values and those predicted by the simulation. This appears to be greater at higher energies. Nevertheless, the measurements agree with the simulation to within about 2.5%. Considering

the uncertainties noted in the above analysis there does not appear to be any compelling evidence to suggest that the simulation is in error. Changing the input paddle thresholds to the simulation, within reasonable values, make less that 0.5% changes in the simulated calibration factors.

The most serious uncertainty in the measurements, as noted in section 4, is the assumption that, when a hit to the NaI is recorded, the inhibit comes up soon enough to prevent photons in later bunches being recorded by the flux monitor. If the inhibit does not come up soon enough, too may flux monitor hits will be recorded which will result in the measured calibration factor being too low.

9 Rate Correction

In an experiment the total number of photons incident on the flux monitor can be found by multiplying the flux monitor counts recorded during the live time of the measurement by the calibration factor f_m. However this is only true at low rates. At normal photon rates a rate correction to the flux monitor counts is necessary because of the fact that the HIGS beam comes in bunches 180 ns apart. When more than one photon is detected in the flux monitor in a single bunch only one will be counted. A rate correction can be calculated using statistics as described in detail in reference [1].

The total number of flux monitor counts during the live time, N_m, is related to the total number of gamma rays during the live time, N_γ, by

$$N_m = Be^{-\epsilon_v(1-\epsilon_m)\frac{N_\gamma}{B}}(1 - e^{-\epsilon_m\frac{N_\gamma}{B}}) \tag{16}$$

where, B is the total number of beam bunches during the live time, ϵ_m is the flux monitor efficiency ($\epsilon_m = 1/f_m$), and ϵ_v is the veto efficiency. This last comes into the equation because it is possible that a photon can cause paddle 1 to fire and thus veto the recording of another photon by the flux monitor.

If photons were the only source of veto paddle hits ϵ_v would be well calculated by the simulation. However it is possible that other interactions not included in the simulation could cause hits in the veto paddle. To investigate this we plot the singles hit rate in each paddle divided by the normal coincidence rate. For the data this ratio is determined directly from the bit pattern register counts for the sample of paddle events for which spectra are recorded. Figures 16 and 17 show this ratio for the data runs taken at 18.5 MeV and 13.0 MeV compared to the simulations at those energies.

It can be seen that the measured paddle rates follow the same trends as predicted by the simulation. However, as we might expect, the measured rates are in general higher that those predicted by the simulation. There is however a significant variation in the relative singles rates from run to run.

For the second week of running we included scalers for the real time and live time gated veto paddle (paddle 1). This was added to the Compton scattering data stream as well. If, during the live time of a measurement, the counts in the veto paddle was N_v, and the flux monitor live-time count is N_m, we find that the ratio N_v/N_γ agrees with the ratios for paddle 1 seen in figure 16, as they should.

We know that, for small photon rates,

$$\begin{aligned} N_m &= \epsilon_m N_\gamma \\ \text{and } N_v &= \epsilon_v N_\gamma \ . \end{aligned} \tag{17}$$

so a first order estimate for ϵ_v can be determined experimentally by using

$$\epsilon_v = \epsilon_m \frac{N_v}{N_m} \ . \tag{18}$$

Therefore, when analyzing the Compton scattering data, we recommend that ϵ_v be estimated using equation 18 for use in equation 16. The fact that this is only a first order

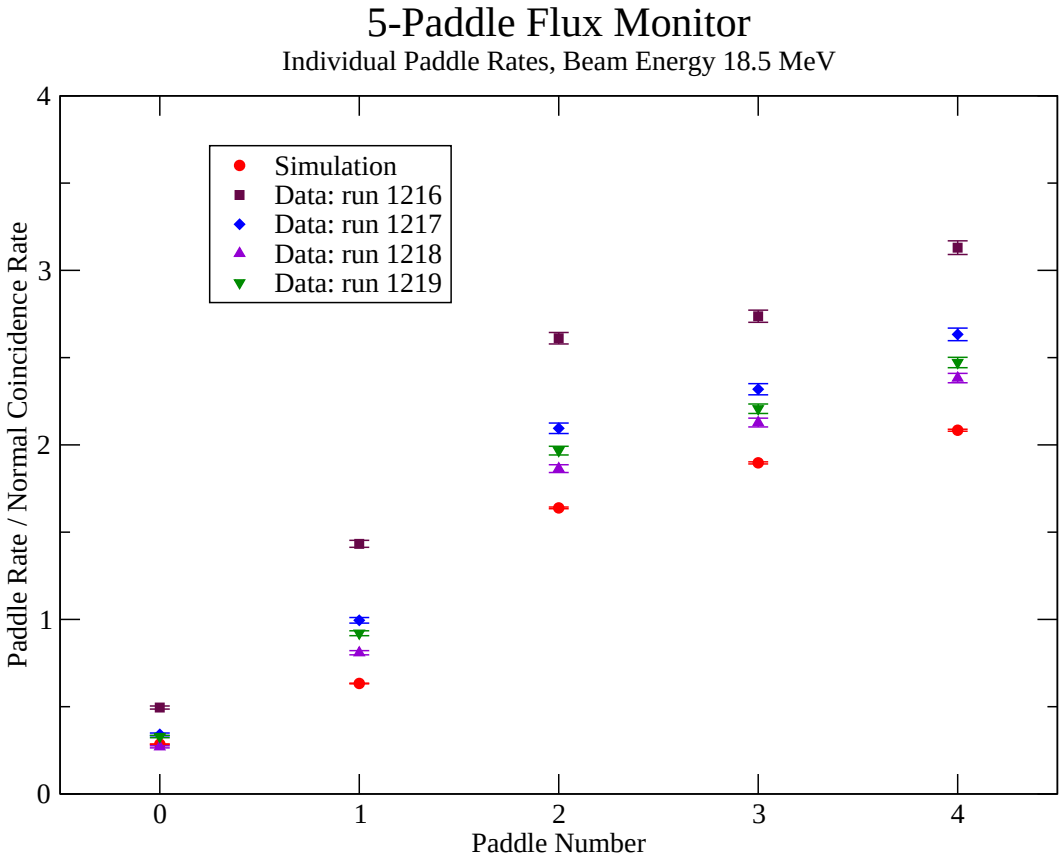

Figure 16: The ratio of the singles counts in each paddle divided by the normal flux monitor coincidence counts. The figure shows the ratio for the data runs taken at 18.5 MeV compared to the simulation at that energy.

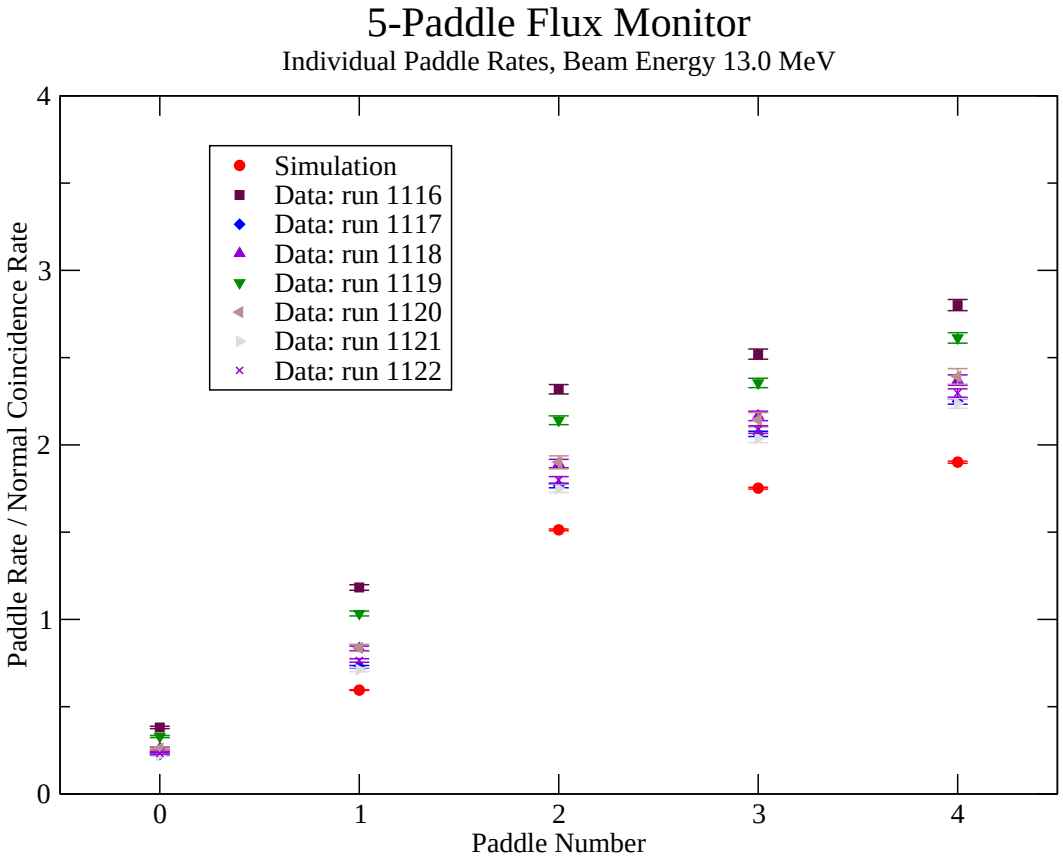

Figure 17: The ratio of the singles counts in each paddle divided by the normal flux monitor coincidence counts. The figure shows the ratio for the data runs taken at 13.0 MeV compared to the simulation at that energy.

estimate for ϵ_v is not too serious since it enters as a second order correction in the calculation of N_γ. For the runs where a live-time scaler for N_v was not available a reasonable guess can be made based on the simulation results and the measurements in the second week of running.

10 Conclusion

Although there are a number of uncertainties in this analysis, our measurements of the flux monitor appear to agree with the simulation to within about 2-3%. Because of the uncertainties in this analysis, there is not enough evidence to suggest that the simulation in not giving a correct description of the flux monitor behavior.

Further work would be needed to verify the performance of the flux monitor to better than 2-3%.

In addition, a dedicated experiment, designed to verify the rate correction given by equation 16 would be advantageous.

A Calibration Running Instructions

Running Instructions for 5-paddle Flux Monitor Calibration

The purpose of these measurements is to

- Provide spectra from the paddles to check that the gains and thresholds for each paddle are stable.
- Provide an inter-calibration between the 5-paddle flux monitor and the Molly NaI detector. This is to check that the efficiency of the 5-paddle flux monitor is consistent with what is predicted by the simulation. As time goes on and we gain more confidence that the simulation is giving the correct efficiency under different conditions, we will hopefully not need to do as many such checks.

Running instructions:

1. Control is from "fluxdaq".
2. Change the prescale for 5-paddle triggers. This is the Phillips 792 Quad Gate and Delay Generator, channel 2 labeled "PRESCALE" in the bottom NIM bin. Change it from the 10 microsecond width setting to the 1 microsecond width.
3. Move the target to "air".
4. Check that the Molly trigger is turned on.
5. Alert the control room operator that we will be putting in some attenuators so they are not surprised by the drop in gamma flux.
6. On the EPICS screen put in at least 4 attenuators.
7. Move Molly into the beam. Watch it move on the "REARVIEW" video screen.
8. Go to the Run Control screen.
9. Start a run.
10. Go to the Scalers screen and check that the "Paddle Live" rate is some between about 10 Hz and 50 Hz and the "NaI Trig" rate is less than about 6000 Hz. If so this a good run. If not, stop the run and change the number of attenuators and try again.
11. We will need to take at least 3, preferably 4, runs at various "Paddle Live" rates within the range 10 Hz to 50 Hz. (Note that the "Paddle Live" is actually the live time counts divided by the real time, so it is not a true live time rate but is a useful quantity to monitor.)
12. For each run we would like to get near about 1% statistics on the number of "Paddle Live" counts (about 10,000). At very low rates of 10 Hz we can stop earlier at about 6000 counts.

13. The rate can be changed for each run by to changing which attenuators are in the beam. Attenuator #1 changes the flux by a factor of 2, attenuator #6 changes the flux by a factor of 4, and attenuators #2, #3, #4, and #5, change the flux by a factor of 10.

14. For each run, record in the log book the Run Number, which attenuators are in, the "Paddle Live" rate and the total "Paddle Live" counts.

15. For one configuration also record a run with the Bismuth (or other target) in the beam to determine the attenuation through that target. This is also a good data point for Paddle calibration measurement. [*Note*: After more careful analysis this last statement proved to be incorrect.]

16. Create root ntupple files for each run. On the Analyzer screen in a terminal window in the directory "/home/coda/experiments/flux/trap" type "./run_main <runnumber>".

17. You can view the spectra from the runs from within root by typing ".L flux_paddle.C+" then "flux_paddle(<runnumber>)".

We will not go into the analysis here, except to mention that the initial goal is to determine the quantity

$$f'_m = \frac{N_{NaI}}{(N_m - B_m T_{live})}$$

where N_{NaI} is the integral of the Molly spectrum, N_m is the flux monitor counts during the live time, B_m is the background count rate from the flux monitor in the live time, and T_{live} is the live time for the measurement. B_m is difficult to measure, hence the need for runs at different rates. Rearranging the above equation we get

$$\frac{N_{NaI}}{T_{live}} = f'_m \frac{N_m}{T_{live}} - N_m f'_m$$

Therefore we plot the Molly rate $\frac{N_{NaI}}{T_{live}}$ against the 5-paddle flux monitor rate $\frac{N_m}{T_{live}}$ and the slope of a linear fit gives f'_m.

References

[1] Rob Pywell, Subatomic Physics Internal Report, SPIR-140, `http://nucleus.usask.ca/technical_reports/report_index.html`.

[2] R.E. Pywell, O. Mavrichi, W.A. Wurtz and R. Wilson, Nuclear Instr. and Meth. A, In press, doi:10.1016/j.nima.2009.04.014

[3] GEANT4 Collaboration, *Nucl. Inst. and Meth. A* 503 (2003) 250.

[4] *Numerical Recipes in C++* Second Edition, W.H. Press, S.A. Teukolsky, W.T. Vetterling, and B.P. Flannery, Cambridge University Press.

[5] V.N. Litvinenko et al, Phys. Rev. Lett., 78 (1997) 4569

[6] D. Murray, et al., *LUCID User's Guide*. `http://nucleus.usask.ca/technical_reports/report_index.html`.